JOURNAL OF AIRCRAFT
Vol. 38, No. 5, September–October 2001

Modeling the Inflation of Ram-Air Parachutes Reefed with Sliders

J. Potvin,* G. Peek,† and B. Brocato‡
Parks College Parachute Research Group, Saint Louis University, St. Louis, Missouri 63103

Sliders are aerodynamic devices designed to reduce parachute opening shock by delaying the canopy spreading stage during inflation. Sliders are used on almost all ram-air parachutes of 1000-ft^2 surface area or less and can be found on an increasing number of round and other cup-shaped canopies. The continued refinement and validation of an inflation model of slider-reefed ram-air parachutes proposed a few years ago by Potvin (*The Aeronautical Journal*, Vol. 101, No. 1007, 1997, pp. 299–313) are reported on. Model validation is accomplished by comparing its predictions with data recently collected from a large number of parachute jumps. The comparison shows good agreement between theory and experiment. Additionally, a series of new scaling laws correlating opening shock and inflation time with descent speed, parachute size, deployment altitude, etc., are derived and discussed.

Nomenclature

A	=	constant defined in Eq. (8)
$a_{\max}$	=	maximum parachute deceleration
$a_{\text{slider}}(t)$	=	slider deceleration
$a(t)$	=	payload deceleration
$C_D(t)$	=	instant parachute drag coefficient
$\langle C_D \rangle$	=	average parachute drag coefficient, $[C_D(0) + C_D(t_f)]/2$
D	=	constant defined in Eq. (8)
F_{friction}	=	friction between the slider and suspension lines
F_k	=	empirical dimensionless factor
g	=	constant of gravity
K	=	parachute spreading rate constant, defined in Eqs. (6) and (7)
L_{chord}	=	fully inflated ram-air parachute chord
L_{line}	=	suspension line length
L_{span}	=	fully inflated ram-air parachute span
L_{thick}	=	ram-air parachute cell thickness or height
m_{slider}	=	slider mass
m_{total}	=	total mass, including parachute and payload
S_f	=	final inflated parachute surface area
S_0	=	parachute surface area just before slider descent
t_{ep}	=	duration of early pressurization
t_f	=	duration of slider descent stage
$t_{\max}$	=	time of maximum deceleration (relative to the beginning of slider descent)
V	=	dimensionless speed, v/v_0
$\dot{V}, \ddot{V}, \dddot{V}$	=	first, second, and third derivatives of the dimensionless speed with respect to dimensionless time τ
v_{ff}	=	payload descent speed before parachute deployment (>0)
v_T	=	terminal descent of the parachute–payload system under a drag area Σ_0 (>0)
$v(t)$	=	payload descent speed (<0)
v_0	=	payload descent speed before slider descent (<0)
W_{total}	=	total weight, including parachute and payload
X	=	slider position relative along the suspension lines, see Fig. 3
Y	=	amount of unfolded canopy span, see Fig. 3
ΔT	=	tension line differential above and below the slider
Ξ	=	dimensionless drag area, $\Sigma g^2/v_0^4$
ρ	=	air density
Σ_f	=	parachute drag area at the end of slider descent
Σ_{slider}	=	slider drag area
$\Sigma(t)$	=	instant parachute drag area, $C_D S$
Σ_0	=	parachute drag area before slider descent
σ	=	length scaling factor
τ	=	dimensionless time, tg/v_0

Presented as Paper 99-1746 at the AIAA/CEAS 15th Aerodynamic Decelerator Systems Conference, Toulouse, France, 8–11 June 1999; received 20 February 2000; revision received 6 October 2000; accepted for publication 9 October 2000.

*Associate Professor, Department of Physics. Member AIAA.
†Consultant, Industrologic, Inc.
‡Research Assistant, Department of Physics. Student Member AIAA.

Introduction

A SLIDER is a device designed to delay the spreading of a parachute during the early stages of its inflation, thereby reducing the amount of opening shock. It is of rectangular shape when used on ram-air parachutes (Figs. 1 and 2) and of circular shape when used on round parachutes.[1,2] A typical slider is made of nylon fabric and nylon webbing and is built to descend the suspension lines freely (Fig. 3). When packed in the deployment bag, it will be placed against the base of the canopy and will delay canopy spreading by virtue of its own drag, which keeps it initially pushed against the bottom of the canopy. The slider moves down the suspension lines only during the final stage of the inflation process when the parachute's inflated volume is large enough to generate the line tension differential that is necessary to push it down (Fig. 3). This device also reduces the rate of canopy spreading itself by traveling down the suspension lines at a relatively slow pace, again due to its own built-in drag. Both effects lead to payload deceleration and slower canopy opening rates, thus generating reduced opening loads. Typically, a slider's surface area is about 1% of that of the fully opened canopy.

Sliders come in two basic versions: first as a sail configuration in which most of its surface area is covered with fabric (Figs. 2 and 3) and second as a pilot-chute-controlled version, which has no fabric cover but is linked via free bridle to the system's extraction chute in order to acquire drag. The main attractive features of sliders are their simplicity of construction and low cost, in contrast to reefing lines that require the use of expensive one-use-only pyrotechnic cutters.[2] Sliders have proven to be the reefing method of choice for countless applications involving ram-air parachutes of surface areas of up to about 1000 ft^2. On the other hand, the use of sliders with cupped- or hemispherical-type parachutes such as round and cruciform parachutes has been a more recent development.[1]

Computer simulation of the aerodynamics of parachute inflation is a very complicated problem.[3] Unlike aircraft, which are rigid structures deflecting air around them, parachutes not only deflect

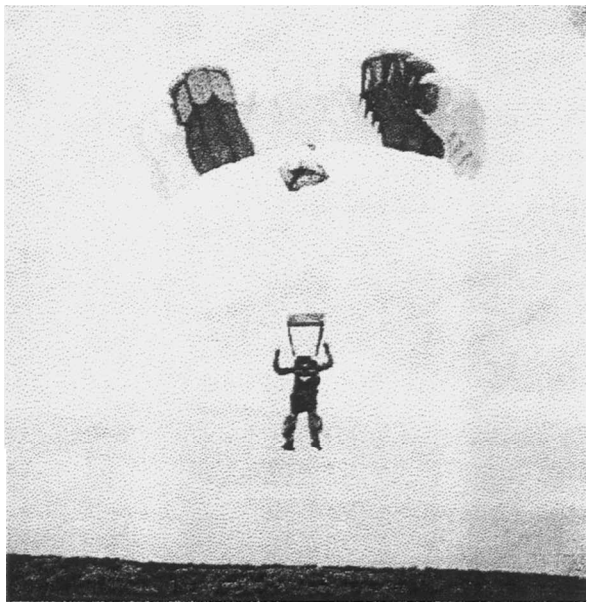

Fig. 1 Flying ram-air parachute with slider shown as the dark-colored rectangle above the jumper's head; parachute risers are shown below the slider.

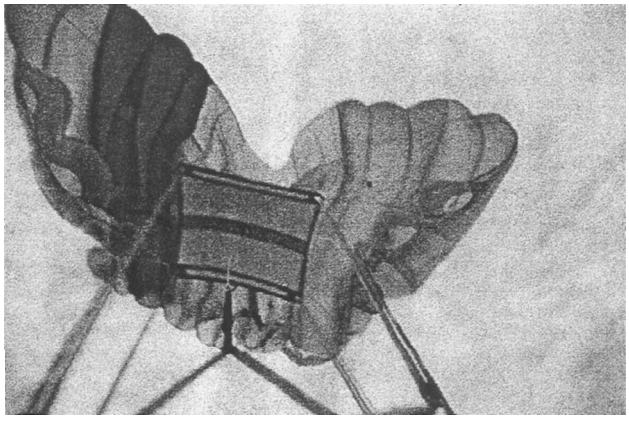

Fig. 2 Inflating ram-air canopy with slider, photographed on its way down the suspension lines; slider is shown as the dark-colored square in the foreground.

air but also adopt shapes dictated by the very airflow that they create. In the case of inflation, parachutes also involve highly turbulent and unsteady flows. Despite all of this complexity, computer simulations of parachute inflation can actually be done with a good degree of accuracy provided that the various stages of inflation are properly identified and that the physics most relevant to each stage is integrated into the model. This not only reproduces the most important peak loads sustained but also provides a good amount of predictive power with little empirical input. Successful simulations of inflating round and other cup-shaped parachutes have been discussed in the literature by Wolf,[4] McVey and Wolf,[5] Macha,[6] Purvis,[7,8] and Potvin.[9]

These detailed models differ from another class of models, which, although based on sound principles, involve an assumed explicit time dependence of the instant opened surface area and shape, or of other variables determined by the explicit payload trajectory.[10–16] In general, these generic models are simpler but do not distinguish between the various inflation phases. Despite their lack of input details, however, they provide good fits of experimental data but will generally have a lack in predictive power given the explicit need for specific time-dependent information.

The ideal parachute model (IPM) is detailed enough to be only applicable to the inflation simulation of parachutes reefed

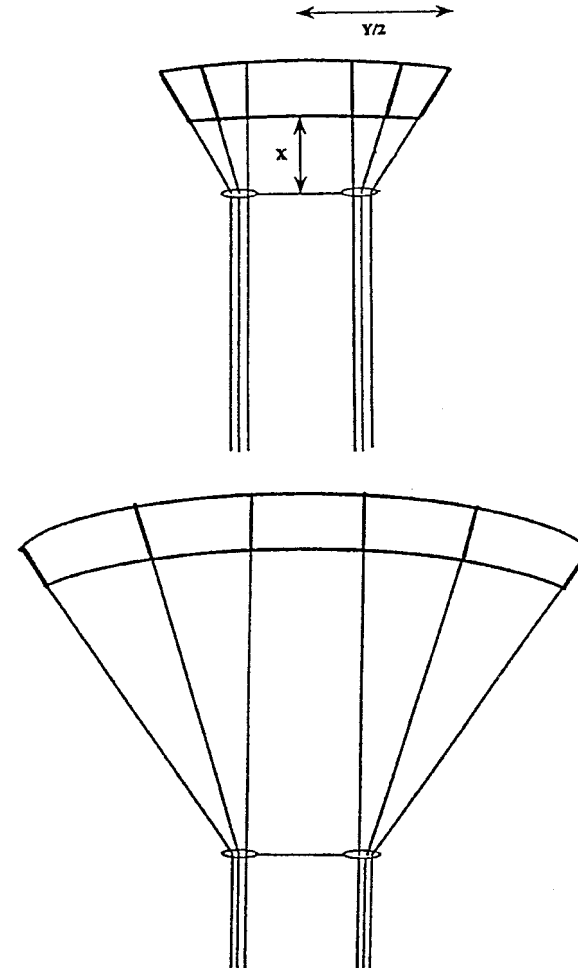

Fig. 3 Sail slider schematics (figure from Ref. 18).

with sliders.[17,18] The IPM represents a second attempt at modeling slider-reefed, ram-air parachute opening after the pioneering work of Lingard[14,19] and has recently been applied to cupped parachutes as well.[20] The IPM is a noncomputational fluid dynamics approach to the study of inflation, being based on the simultaneous solution of the equation of motions of the payload and slider.

Various predictions of the IPM have already been compared with experiments[18] and have been found to be consistent with the latter within fairly large error bars. The first goal of this paper (and of its conference version[21]) is to present our latest attempt at validating the model using new and improved parachute riser load data recently collected from over 60 test jumps on ram-air canopies of different designs, sizes, and wing aileron trim settings. The second goal is to present a new series of scaling laws that relate maximum deceleration and time of maximum acceleration to parachute and initial trajectory parameters. [Note erratum of Ref. 18: Figure 4b should be plotted vs $-\ell n(t_{\max} g/v_0)$ rather than $\ell n(t_{\max} g/v_0)$ as claimed; also Eq. (17) is incorrect and should be $R_f = t_f g/v_0 = 2g\Sigma_0^{1/4}(\sqrt{\Sigma_f} - \sqrt{\Sigma_0})^{1/2}/v_0^2 K$.] [Note erratum of Ref. 21: Equations (2.11) and (4.4) are incorrect and should be replaced by Eqs. (16) and (20) of this paper, respectively; as a consequence, Tables 4.2 and 4.3 contain errors.]

Review of the IPM

Four Stages of Slider Reefing Inflation

Accurate inflation modeling demands that the physics involved be as detailed as possible, which can be done by first distinguishing the various deployment and inflation phases involving different hardware, fabric components, and forces at play. Most slider-reefed parachutes deploy and inflate in four stages, which are, in order of occurrence, line stretch, bag strip, early pressurization, and slider

descent (or canopy spreading). During line stretch, the suspension lines are first deployed and stretched, whereas during bag strip the parachute is extracted out of the container bag but remains in a limp state. This last stage is followed by initial pressurization, which marks the instant at which the parachute begins to pressurize and inflate into a temporary shape. During early pressurization, the slider remains pushed against the base of the canopy because of its own drag. At this point the parachute–payload system begins decelerating substantially. The inflation process ends with the slider descending the suspension lines to allow full spreading of the canopy. This is the stage that is described by the IPM. Maximum loading is expected to occur during the slider descent phase because a parachute's surface area becomes the greatest during that stage. Indeed, this is confirmed by our new database for parachutes of surface area of 200 ft^2 or less. However, the database also shows that larger ram-air parachutes and most cupped parachutes instead exhibit maximum loading during early pressurization. Clearly, a large enough amount of exposed canopy coupled to a high payload descent rate can cause the highest loading to occur before slider descent. For this reason, the IPM allows for the calculation of opening shock only for the smallest of canopies.

Assumptions and Evolution Equations

The IPM is formulated through the simultaneous use of the equations of motion of both payload and slider. The model is also supplemented by an extra equation based on the amount of unfolded parachute surface area being directly correlated with the location of the slider along the suspension lines (Fig. 3). The articulation of these three ingredients is specific enough to yield different evolution equations for ram-air parachutes and cupped-type parachutes.[20] In what follows we refine and further justify the approximations that were originally presented in Ref. 18 to construct the basic evolution equations.

The IPM is based on a series of approximations, four of which are as follows.

First, it is assumed that the payload's descent is vertical during deployment. Additionally, vertical descent is assumed to continue until the very end of inflation. This is borne out of a large number of observations that show the extraction pilot chute always trailing straight above the canopy rather than flying behind it as it would be during the glide phase. [On sport canopies, the pilot chute is connected to a long bridle anchored to the top of the parachute (Fig. 1).]

The absence of lift is a second approximation and follows from the first. Because the parachute does not fly during inflation, there is no lift force. Also the drag force continues to point upward.

The third approximation concerns unsteady drag coefficient and apparent mass effects: By design parachutes decelerate at rates that are large enough to warrant a time-dependent drag coefficient. Studies of cup-shaped parachute opening by Knacke,[2] Strickland and Macha,[22] and Ludtke[23] indicate that, compared to its steady-state value, the instant value of the drag coefficient C_D during the spreading phase increases with time by factors of 1.5–2.0. This should be expected for ram-air wings as well, given the similarities of the overall airflow around all inflating shapes. Unlike cup-shaped parachutes, however, we expect the inertial effects of the air trapped inside ram-air canopies to be unimportant given the small volume of the cells that enclose the air (Fig. 1). Indeed, comparing the weight of the air trapped inside an inflated ram-air wing of typical surface area ($S_f \approx 200$ ft^2) and cell thickness ($L_{\text{thick}} \approx 1$ ft) with that of a 200 lb load at 4000-ft mean sea level (MSL) would give a weight ratio of order $W_{\text{tot}}/\rho S_f L_t g \sim 15$, that is, two orders of magnitude from being numerically important. The combination of explicitly assuming a time-dependent drag coefficient and little enclosed air leads one to disregard altogether the so-called apparent mass terms in the parachute drag force. This contrasts with the studies of cup-shaped parachutes, which use a (constant) steady-state drag coefficient together with a time-dependent apparent mass term into the payload equation of motion to account for both effects.[4–6,24–34]

The fourth approximation is that there are harmonic forces from the suspension lines and risers: The springlike properties of the suspension lines and harness risers are left out as well. The suspension line natural frequencies that arise from the loading conditions typical of manned parachute use are at least 10 times higher than the basic frequencies associated with ram-air inflation itself. Such frequencies are, thus, high enough to permit the complete propagation of the parachute drag force down the suspension lines and risers and to the payload in a timescale that is much smaller than that of inflation. Although such line and riser springlike behavior will be visible on the measured force data, it will not substantially change the overall shape of the force evolution over the relevant timescales.

These four approximations mean of course that the equation of motion for the payload can be written simply in terms of the total weight W_{tot}, the parachute drag area $C_D(t)S(t)$, and the basic drag equation as

$$m_{\text{total}} a(t) = \tfrac{1}{2}\rho C_D(t) S(t) v(t)^2 - W_{\text{total}} \tag{1}$$

where $v(t)$ is understood to be negative. This equation is supplemented with the equation of motion of the slider, which can be expressed in terms of slider drag, line tension differential ΔT below and above the slider, and line friction F_{friction}:

$$m_{\text{slider}}\, a_{\text{slider}} = \tfrac{1}{2}\rho \Sigma_{\text{slider}} v(t)^2 - \Delta T + F_{\text{friction}} \tag{2}$$

As discussed in detail in Ref. 18, Eq. (2) incorporates other approximations such as that of a negligible slider weight and of the replacement of slider speed in the drag equation by the payload speed. Here Σ_{slider} would be the slider's drag area, which should be about twice its steady-state value because of the slider's quick acceleration down the suspension lines.

Reference 18 also discusses that ΔT and F_{friction} being directly correlated to total drag can be written as products of $C_D(t)S(t)v^2(t) \equiv \Sigma(t)v^2(t)$, an observation that brings another important simplification, namely the slow opening, quick deceleration approximation: In relation to the final and initial values of the speed and drag area, it is assumed that the change of the square of the velocity is much larger than that of the drag area, namely,

$$\frac{\Sigma_f - \Sigma_0}{\Sigma_0} \ll \frac{v_0^2 - v_f^2}{v_f^2} \tag{3}$$

These assumptions lead to rewriting Eq. (2) as

$$m_{\text{slider}} a_{\text{slider}} = \text{const} \cdot v(t)^2 \tag{4}$$

where $\Sigma(t)$ is replaced by a constant of order $\approx(\Sigma_0 + \Sigma_f)/2$.

The last ingredient of the IPM consists in expressing the parachute instant drag area $\Sigma(t)$ in terms of the location of the slider $X(t)$ along the suspension lines as shown in Fig. 3, namely,

$$\Sigma(t) = C_D(t)S(t) \approx C_D(t) L_{\text{chord}} Y(t) \approx C_D(t) X(t) \frac{L_{\text{chord}} L_{\text{span}}}{L_{\text{line}}} \tag{5}$$

The evaluation of this equation involves the last major assumption, namely, that of slow drag coefficient increase rate: Past experimental studies on round parachutes[2,22,23] suggest that during the same time interval the increase in $C_D(t)$ is much smaller than that of the normalized wing span $X(t)/L_{\text{line}}$, namely, by factors 1.5–2.0 and 10.0, respectively on typical aspect ratio ram-air wings. This assumption allows the calculation of the second time derivatives of Eq. (5) while using $C_D(t) \approx \langle C_D \rangle = [C_D(0) + C_D(t_f)]/2$ and solving for $a_{\text{slider}} = \mathrm{d}^2X/\mathrm{d}t^2$. This gives

$$\frac{\mathrm{d}^2 \Sigma(t)}{\mathrm{d}t^2} = K v(t)^2 \tag{6}$$

The so-called canopy spreading rate constant K is dimensionless and proportional to several parachute construction characteristics[18]:

$$K \propto \frac{\langle C_D \rangle \rho L_{\text{chord}} L_{\text{span}} \Sigma_0}{2 F_K m_{\text{slider}}^{\text{total}} L_{\text{line}}} \tag{7}$$

Here F_K is a nondimensional factor to be determined empirically. For manned-type openings, it has a value approximating 50. In a

Table 1 List and brief description of the ram-air parachutes flight tested[18,36–39]

Model	Number of load-bearing cells	Surface area, ft^2	Modifications	Manufacturer
Goliath/MC-4	9	360	Standard	Para-flite
Cruislite	7	220	Standard	Para-flite
Evolution	23	240	Standard	Para-flite
Stiletto	9	150	Standard and heavy slider	Performance designs
Sabre	9	120	Standard, long and short brake settings	Performance designs
Sabre	9	150	Standard, long and short brake settings	Performance designs
Sabre	9	230	Standard, long and short brake settings	Performance designs
Trilobe	7	320	Standard	Quantum parachutes

sense, F_K represents effects not yet included in the model, such as parachute fabric stiffness,[35] suspension line and riser stretching, etc. Moreover, F_K is likely to include a nondimensional correction to Eq. (5) that relates slider position along the suspension lines to the actual amount of opened canopy surface area. However, it will be shown that despite the uncertainty surrounding F_K, the IPM can make several useful predictions without the explicit knowledge of K or F_K, particularly with regards to scaling.

Thus Eqs. (1) and (6) define the IPM, together with the parameter inputs related to the trajectory before slider descent, that is, w, ρ, and v_0, and the parachute construction characteristics K, Σ_0, and Σ_f. The values of w and ρ are easily measured in the laboratory; on the other hand, v_0, K, Σ_f, and Σ_0 are calculated as explained in the following sections. These equations can be solved numerically to yield the basic time evolution of the payload fall rate, acceleration, and canopy surface area.

Comparing the IPM with Experimental Data

The first effort at validating the IPM involved the use of riser load data collected at a low sampling rate (10 Hz) and on two of the four parachute risers that connected the payload to the parachute suspension lines.[18,36] This incomplete data gave accurate inflation times, which could be compared unambiguously with the predictions of the IPM. However, assumptions were needed to infer the value of total drag. Moreover, assumptions were also needed to estimate descent rate at the beginning of the slider descent phase, v_0. In an effort to generate better quality data, the test jumpers of the Parks College Parachute Research Group have performed over 60 jumps using much higher sampling rates (up to 1000 Hz) on measurements performed on all four risers. Moreover, an electronic barograph was used to attempt to measure the descent rate at line snatch time to provide data for a calculation of v_0. As discussed in more detail in Refs. 36 and 37, the barograph, load cells, and data acquisition system were built from standard designs using off-the-shelf sensor and electronic components.

To address questions of size scaling and opening shock for various parachute designs, this new database includes the study of over 15 configurations defined by the following parameters: number of cells (7–23 cells), total surface area (120–360 ft^2), slider weight (0.5–5.0 lb), and aileron trim (deep to shallow). These configurations are listed in Table 1. The so-called aileron trim configurations consist in changing the amount of what parachute riggers call brake setting. Such settings are temporary and rigged for the inflation phase only. They are implemented by shortening or lengthening the actual length of the suspension lines used for steering during the glide. Effectively, brake settings amount to adjusting aileron deflection on the backside of the parachute wing. Brakes settings are used to cancel the forward surge that many ram-air wings experience toward the end of inflation. They are also used to reduce opening shock. Here standard setting correspond to the aileron deflection installed in production whereas long brake settings configurations corresponds to an aileron deflection that is smaller than the standard setting. A short brake setting configuration corresponds to an aileron deflection that is larger.

All of these parachute configurations were deployed at 4000-ft MSL following a vertical, belly-to-Earth, and 5-s free-fall at a terminal velocity of about 176 ft/s. Most deployments were initiated with the same 31-in. hand-deployed pilot chute system. All canopies were flown under similar weight conditions in the 200–220 lb suspended weight range.

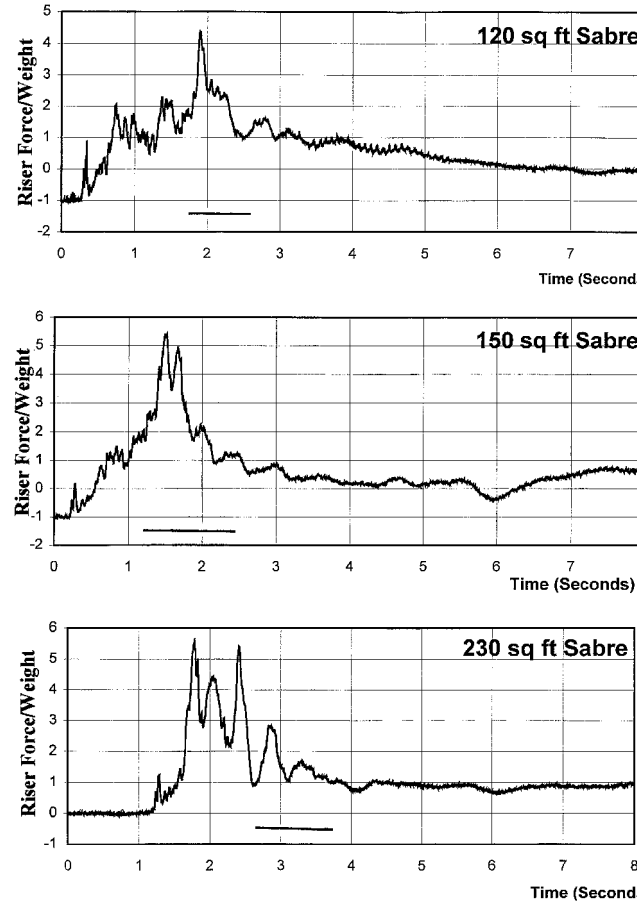

Fig. 4 Time evolution of the total riser force sustained by three Performance Designs parachutes: horizontal line below the peaks marks the slider descent stage.

Sample Riser Loads Curves: General Remarks

Figure 4 shows the time evolution of the total riser force measured on Performance Designs Sabre canopies of 120-, 150-, and 230-ft^2 surface area. The small peak on the left side of each graph corresponds to the so-called snatch force that arises when the suspension lines have deployed and the canopy has extracted out of its deployment bag. On the other hand, slider descent is indicated by the bottom horizontal line that corresponds to the signal generated by a hand switch triggered by the test jumper on witnessing the descent of the slider. These data show that the slider descent stage is characterized by the highest loads sustained on the smaller canopies, namely, the 120- and 150-ft^2 Sabres. In contrast, larger

canopies such as the 230-ft^2 Sabre experience the highest load during the bag strip or early pressurization stages. This trend is because a large parachute releases much more canopy fabric at bag strip and at higher descent speeds, thus generating significantly more drag. Finally, the onset of glide is visible on all three canopy sizes shown and corresponds to the smooth double hump structure that follows the jagged slider descent peak.

Not shown in Fig. 4 is that the loading measured on each parachute riser is uneven throughout the inflation sequence.[36,38] In particular, the rear risers take most of the load during inflation, whereas the front risers sustain more force at the onset of canopy glide.

Finally, the riser load data feature 4–8 Hz fluctuations modulating the overall evolution curve. The main sources for these variations are as follows: 1) the variations in the instant inflated volume of each cell that occur during the early stages of inflation, as caused by the partly stochastic nature of the filling process (see Fig. 3) and 2) the small-scale horizontal motions of the canopy that result in violent back-and-forth rocking of the canopy, themselves caused by fluctuations in canopy trim or by air temporarily trapped under the canopy and spilling to one side. Such fluctuations provide the driving force causing the suspension lines and risers to oscillate axially. The payload loading that results is analogous to that of a mass sustaining a constant force while being attached to a spring. In the case of an undamped spring, the spring force increases to up twice of that of the external force applied (if the mass has started from rest). For a damped spring, the maximum spring force could still exceed that of the applied force, but to a lower value.

Input Parameters

Descent Speed Before Canopy Spreading

It has long been known that parachute opening shock is very sensitive to the payload's descent speed at the beginning of inflation. Most often, large variation in opening shock on a drop-to-drop basis will be caused by speed variations that occurred during deployment, line stretch, or bag strip. Our new database shows that v_0 is rarely equal to the known deployment speed as assumed in Ref. 18 because of the significant duration of the deceleration generated during early pressurization. However, v_0 cannot be measured accurately with current barograph-based technology given that the latter provides only speeds averaged over timescales that are greater than the entire duration time of slider descent.

Our approach is to estimate v_0 with a formalism that takes into account payload deceleration before slider descent. The basic formula is obtained by directly integrating the equation of motion for the case of the payload falling under a partly opened parachute of constant drag area Σ_0 (Ref. 36). The resulting formula thus expresses v_0 in terms of the barograph measurement of the parachute-load system at the onset of deployment, namely, v_{ff}, and the duration of early pressurization, that is, t_{ep}, as estimated from the riser loading time evolution graphs or from video. It is given by

$$v_0 = v_T \left(\frac{1 + A \exp(-v_T t_{ep}/D)}{-1 + A \exp(-v_T t_{ep}/D)} \right) \tag{8}$$

where $D = m/(\rho \Sigma_0)$, $A = (-v_{ff} + v_T)/(-v_{ff} - v_T)$, and $v_T^2 = 2W/(\rho \Sigma_0)$; moreover, $v_0 < 0$, $v_{ff} > 0$, and $v_T > 0$. Here v_T would correspond to the terminal fall speed of the payload when the canopy is opened at a (fixed) drag area Σ_0.

Values for S_0 and Σ_0 are calculated using photographs of the parachute during early pressurization from the jumper's perspective. Such photographs usually show the parachute initial surface area S_0 superposed to the outline of the slider that is usually pushed against it. Relative to the known slider surface area, S_0 is typically five to eight times larger. For example, based on a decelerating flat plate approximation ($C_D \approx 1.5$–2.0) Σ_0 is then estimated at ≈ 20 and ≈ 25 ft^2 for the Sabre 120 and 150 canopies, respectively.

On the other hand, the value of the early pressurization time t_{ep} can be measured by calculating the time difference on a riser load evolution graph between the locations of the snatch force peak and of the beginning of the slider-descent peak.[36] The latter event is tagged by the signal of the test jumper hand switch discussed earlier as shown by the horizontal line in Fig. 4. (In the absence of hand switch data, the slider descent peak can be identified by comparing the peaks of the riser load graph with the slider descent time as measured on video.[36]) However, such a tag may suffer from a significant error caused by the test jumper's swiftness, or lack of thereof, at triggering the switch. For small canopies, a better approach is to locate the beginning of the tallest and most prominent peak in the riser load graph.[36] In principle, the value of t_{ep} depends on the specifics of the canopy design, including the size and angle of the cell inlet, chord length, etc. In the case of the Performance Designs Stiletto 150, for example, t_{ep} is long enough to allow a deceleration to speeds that are lower than the deployment speed by as much as 20–30% (Ref. 36). Again note that Eq. (8) is only an approximation because it depends on the assumption of a constant parachute drag area during early pressurization.

Final Drag Area Σ_f

The numerical solution of the IPM ends when the drag area reaches the value specified by $\Sigma_f \equiv C_D(t_f) S_f$, an input to the computer program. The value of S_f is given by the product of the span and chord, as supplied by the canopy manufacturer. The values of $C_D(t_f)$, on the other hand, is taken to be in the range of 2–3 as suggested by the studies mentioned earlier.[4–6,22] As will be shown, such a high final drag coefficient happens to terminate the simulations at the point where the parachute begins to glide.

Canopy Spreading Rate Parameter K

The proper use of the IPM for comparison with experiment begins with the determination of the K factor appearing in Eq. (6). As discussed earlier, such a number is difficult to calculate accurately. This may not be a problem, however, given the weak dependence that variables such as maximum deceleration a_{max} and time of maximum deceleration t_{max} have on K, namely, $\approx K^{\pm 1/3}$, as shown in the next section. Here we take advantage of the fact that many repeat jumps were performed for each parachute configuration tested: By the use of the data of one jump chosen as the reference jump, a value of K is obtained by matching the IPM to it. The same value is then used in the analysis of the other test jumps of the parachute configuration under consideration.

Theory Meets Experiment

Figures 5–8 show both theoretical and experimental time evolutions of payload acceleration, as calculated from the total load measured on the risers and as displayed on a jump-to-jump basis. The theoretical curve is compared to the slider descent portion of the experimental curve given that the IPM describes only this inflation stage. The data come from the flight testing of the Sabre 150 and Sabre 120, which, as explained earlier, display a dominant peak during slider descent by virtue of their small size. For each canopy, Figs. 5–8 show the data for two brake settings. The experimental acceleration is calculated from the total force sustained by all four risers and sampled at a rate of 1000 Hz.

Figures 5–8 show good agreement between theory and experiment on most of the single-jump curves displayed. By good agreement we mean that the IPM curve is matching well the basic envelope of the experimental curves by going through each local fluctuation at (approximately) midamplitude. Figures 5–8 show some of the best agreements as well as the worst, where the theory is systematically overestimating the acceleration at the end of slider descent by 1 g or more. In general, comparing the IPM with the entire database indicates a good match for about 80% of the 60 jump-to-jump curves so far analyzed. What is most remarkable is that, for each parachute configuration studied, such a good match is based on a drop-to-drop change of v_0 while keeping fixed the values for K, ρ, Σ_0, Σ_f, and W. As discussed before, such changes of the initial speed are due to variations in the duration of the early pressurization stage so typical of ram-air parachute inflation.[39]

Comparing the values of K computed in Ref. 18 with those obtained here, we note that the latter tend to be greater than the former

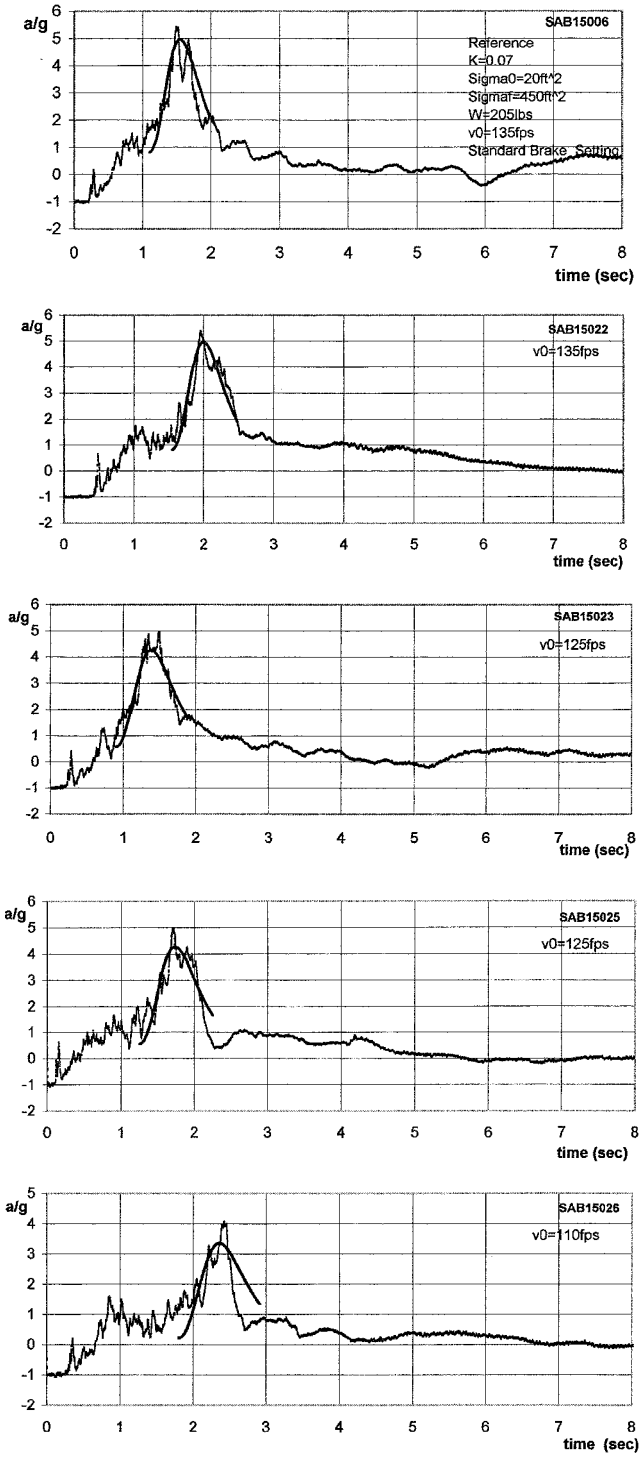

Fig. 5 Payload deceleration (in gravitational acceleration) vs time (in second): Performance Designs Sabre 150 parachute with standard brake setting.

by almost a factor of two in the case of the smaller canopies. This is because v_0 is overestimated whenever $v_0 \sim v_{ff}$ is assumed, as was done in Ref. 18. In most deployments, payload speed before slider descent is always substantially lower.

Ram-Air Parachute Inflation Scaling Laws

Having validated the IPM to a good accuracy allows us to explore several of its most useful predictions, namely, the derivation of scaling relationships that correlate maximum deceleration and inflation time with relevant parachute parameters and deployment characteristics. As shown in Ref. 18 and in the subsequent paragraphs, this can be achieved by numerically solving the IPM

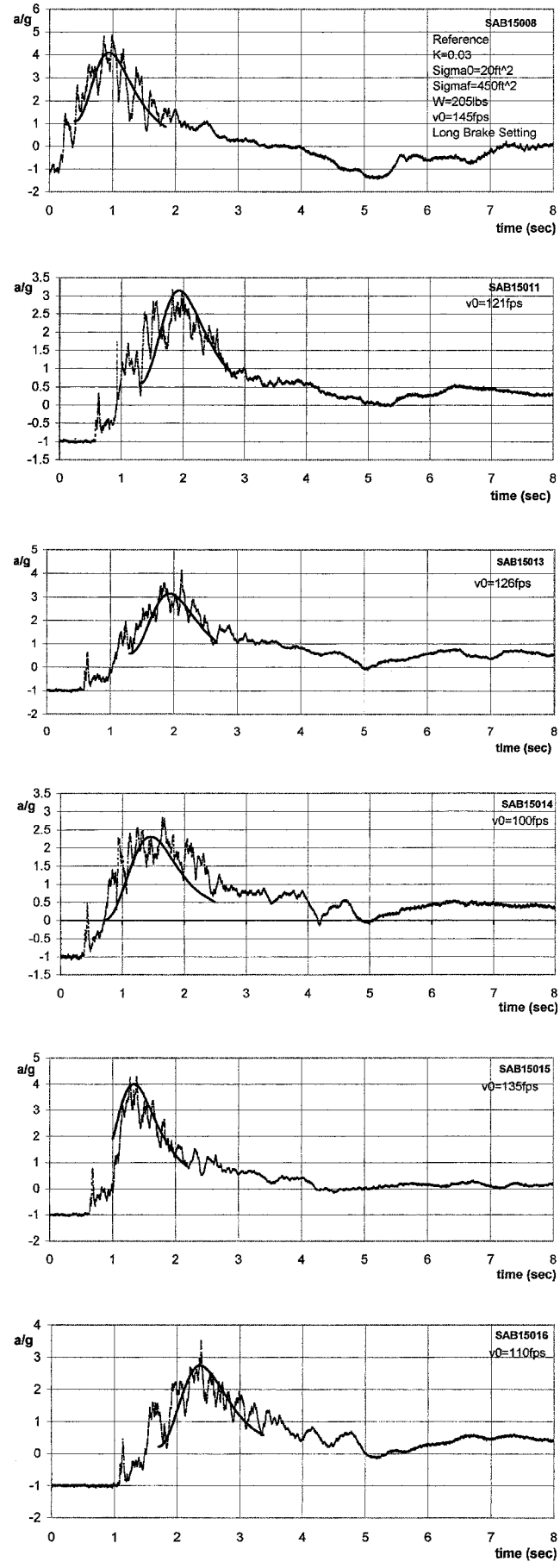

Fig. 6 Payload deceleration (in gravitational acceleration) vs time (in second): Performance Designs Sabre 150 parachute with long brake setting.

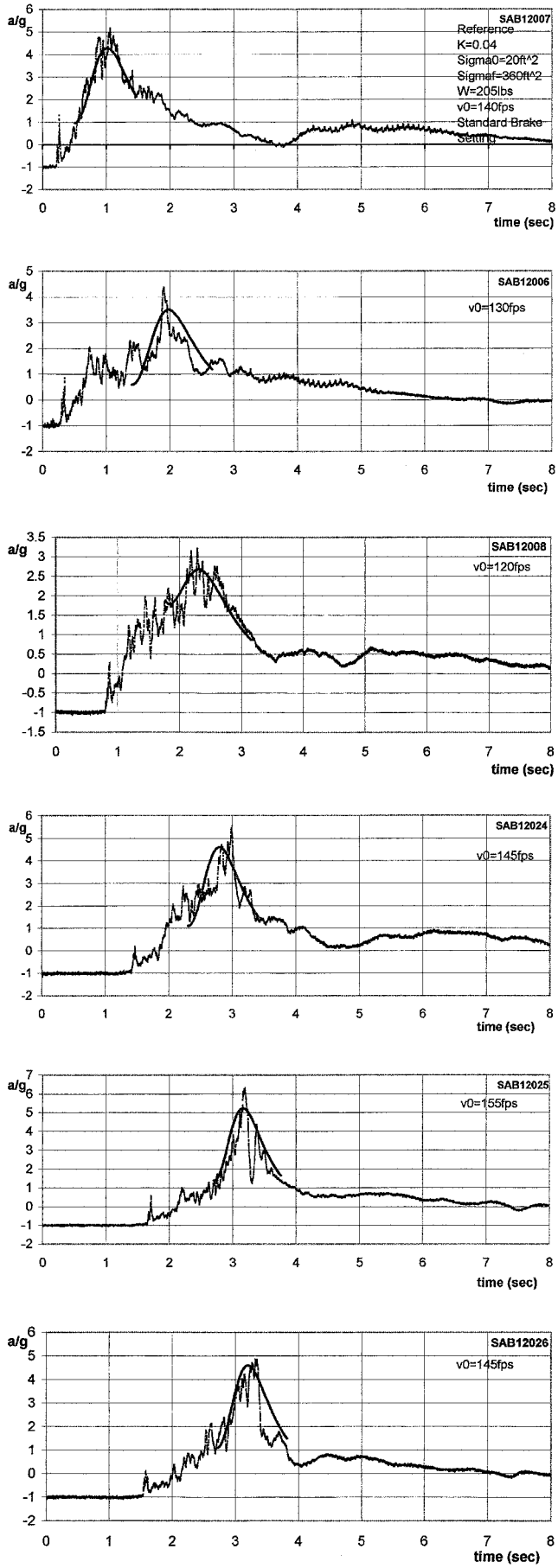

Fig. 7 Payload deceleration (in gravitational acceleration) vs time (in second): Performance Designs Sabre 120 parachute with standard brake setting.

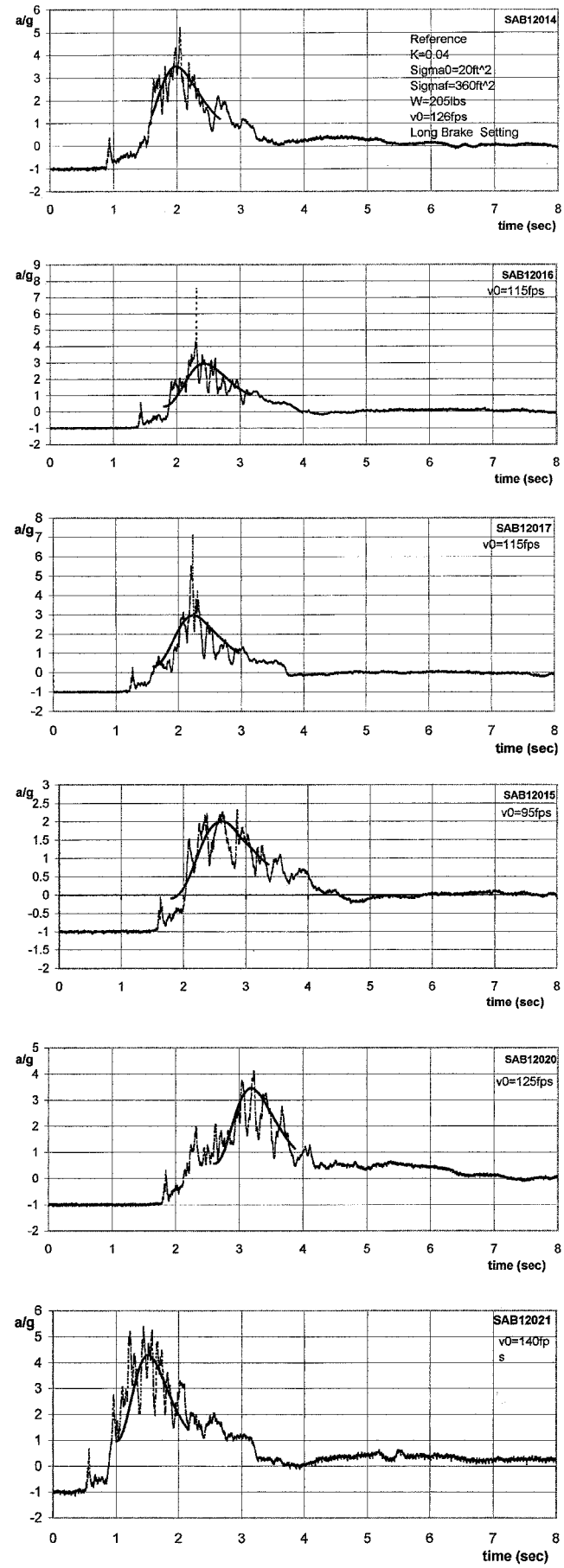

Fig. 8 Payload deceleration (in gravitational acceleration) vs time (in second). Performance Designs Sabre 120 parachute with long brake setting.

for thousands of different parachute component sizes, deployment speeds, and deployment altitudes and analyzing the resulting data in the appropriate way.

Review of Basic IPM Scaling

Reference 18 shows how to obtain two very general scaling laws from the combined solution of Eqs. (1) and (6). This is done first by rewriting these equations in terms of the following dimensionless variables: $\tau = tg/v_0$, $V = v/v_0$, $\Xi = \Sigma g^2/v_0^4$, $\dot{V} = \mathrm{d}V/\mathrm{d}\tau$, $\ddot{V} = \mathrm{d}^2V/\mathrm{d}\tau^2$, and $\dddot{V} = \mathrm{d}^3V/\mathrm{d}\tau^3$. Combining these dimensionless versions of Eqs. (1) and (6) to eliminate the drag area gives the following differential equation, which completely defines the time evolution of the descent rate $V(\tau)$:

$$R_p V^6 = V^2\dddot{V} + 6\dot{V}^3 - 6V\dot{V}\ddot{V} + 6\dot{V}^2 - 2V\ddot{V} \tag{9}$$

Here R_p is a dimensionless ratio defined by

$$R_p = \frac{\rho K v_0^6}{2W_{\text{total}}\, g^2} \tag{10}$$

This is an interesting result, which shows how parachute and deployment characteristics determine the rate of change of the dimensionless speed through the values of R_p and through the dimensionless final drag area $\Xi_f = \Sigma_f g^2/v_0^4$, which specifies the end of the evolution.

This result also suggests that variables describing events before final time t_f should be dependent on R_p only. This applies in particular to the maximum deceleration $a_{\max}$ and to the time of maximum deceleration, $t_{\max}$. This observation was confirmed by thousands of IPM simulations carried out at various values of parachute and deployment variables, the results of which are graphed in Fig. 9. Fitting the numerical data to a straight line yielded[18]

$$a_{\max}/g = 0.360R_p^{0.332} \tag{11}$$

$$t_{\max} g/v_0 = 1.532R_p^{-0.354} \tag{12}$$

Using v_0 and $a_{\max}$ as inputs, our old and new inflation database suggests typical values of R_p to be in the range of 1000–3000 for the manned-type canopies studied. Also note the following.

1) Maximum acceleration and time of maximum acceleration do not depend on the value of the final drag area Σ_f as expected because $a_{\max}$ mostly occurs near the half-point of the slider descent stage when the parachute is partially opened (exceptions are shown in Ref. 17).

2) Maximum $a_{\max}$ and $t_{\max}$ are highly sensitive to v_0, which should also be expected.

3) The weak dependence on K, that is, $\sim K^{\pm 1/3}$ helps in the validation of the IPM given its uncertain value.

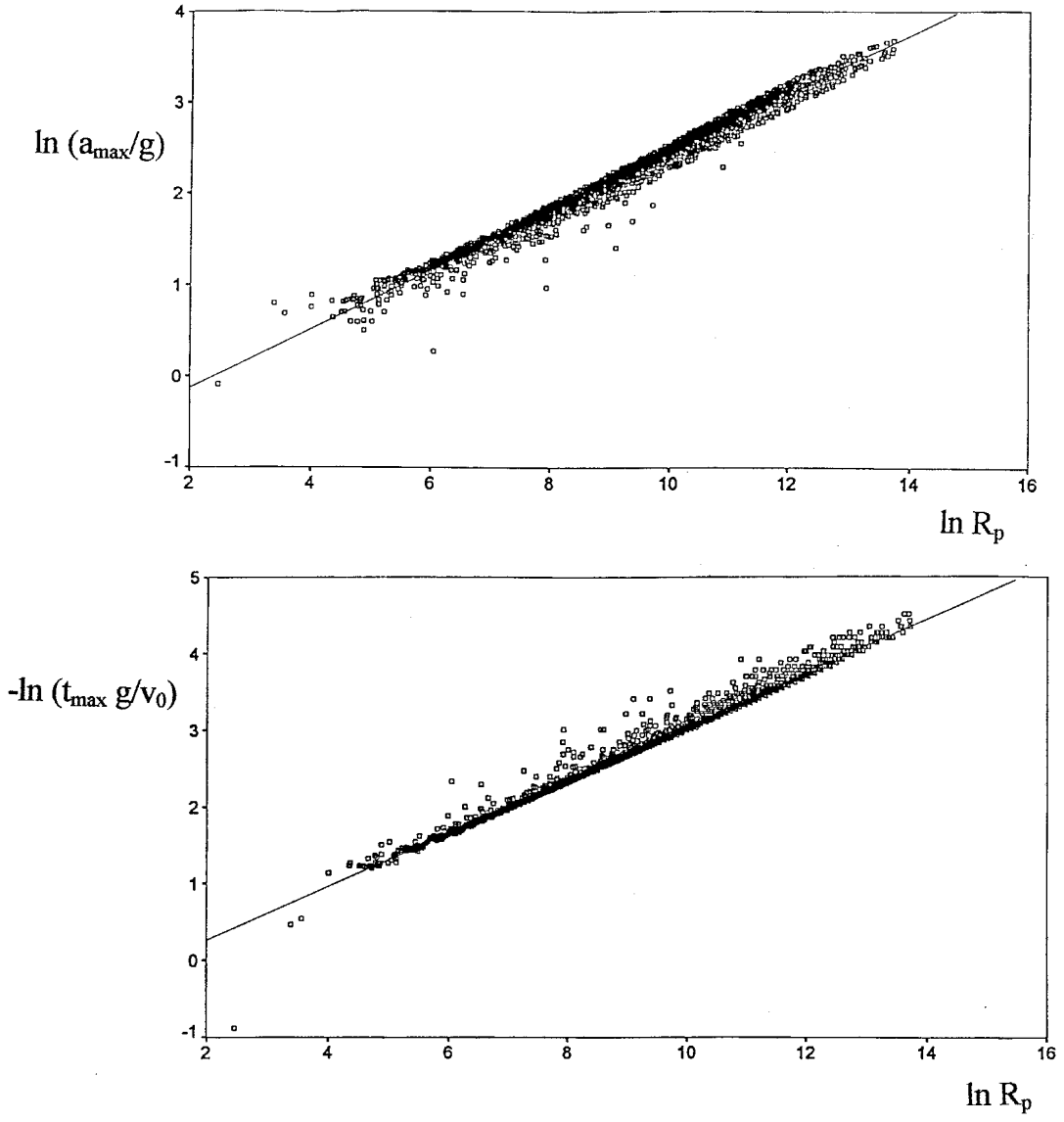

Fig. 9 Maximum deceleration and time of maximum deceleration as obtained from numerical solution of the IPM over 2000 designs[18]: numerical data plotted against the dimensionless ratio R_p defined in Eq. (10) (data from Ref. 18).

4) Equations (11) and (12) can be combined to yield another very powerful result, which can be useful in organizing data collected on a large number of different parachutes, namely,

$$v_0 = 1.81 R_p^{0.022} a_{\max} t_{\max} \approx 2.2 a_{\max} t_{\max} \tag{13}$$

the second equality obtained by assuming $R_p \sim 1000$–$10{,}000$, a range typical of sport canopies.[17,18] We refer to Eq. (13) as IPM scaling. This result simply shows a long-known fact that parachutes that open the hardest also have the shortest inflation time.

Finally note that, strictly speaking, $a_{\max}$ is the maximum deceleration of the payload during the slider descent phase of ram-air wing inflation. Only in the case of small canopies does $a_{\max}$ correspond to the largest deceleration, that is, opening shock, sustained by the payload during the entire inflation sequence.

New Scaling Laws

Scaling with respect to the change of selected parachute design or deployment input values can now be derived.

Size Scaling

Changing the size of a given parachute design has repercussions on the canopy spreading rate constant K as well as on $a_{\max}$ and $t_{\max}$. Looking at Eq. (7) suggests that a change of all construction lengths by a factor σ results in

$$K_{\text{new}} \propto \sigma^3 K_{\text{old}} \tag{14}$$

which propagates into Eqs. (11) and (12) as

$$\left(\frac{a_{\max}}{v_0^{1.992}}\right)_{\text{chute2}} = \sigma \left(\frac{a_{\max}}{v_0^{1.992}}\right)_{\text{chute1}} \tag{15}$$

$$\left(\frac{t_{\max}}{v_0^{-1.124}}\right)_{\text{chute2}} = \frac{1}{\sigma^{1.06}} \left(\frac{t_{\max}}{v_0^{-1.124}}\right)_{\text{chute1}} \tag{16}$$

The size scaling of $a_{\max}$ and $t_{\max}$ can be established once the size scaling of v_0 is known. In this regard, the IPM predicts two types of size scaling depending on whether the opening is one of two categories: 1) nominal, that is, when the opening sequence evolves through early pressurization and canopy spreading of finite duration, and 2) instant, that is, when early pressurization is almost instantaneous, for example, when caused by the premature release of the canopy before line stretch as during the so-called line dumps. In the case of instant openings, one has the following scaling law given that $v_0 \approx v_{ff}$:

$$(a_{\max})_{\text{chute2}} = \sigma \cdot (a_{\max})_{\text{chute1}} \tag{17}$$

$$(t_{\max})_{\text{chute2}} = \sigma^{-1.06} \cdot (t_{\max})_{\text{chute1}} \tag{18}$$

Interestingly, Eq. (17) suggests that instant openings should give higher opening shocks on large parachutes than small ones. Given the rarity of instant openings, the current size of the database prevents any meaningful experimental check of this result.

Regarding nominal openings, Eqs. (15) and (16) depict a more complex picture where scaling down in parachute size reduces the rate of canopy surface opening [see Eq. (14)] while it increases the value of the initial velocity v_0. The latter observation follows from Eq. (8) and occurs because smaller canopies feature a shorter early pressurization time and a faster terminal descent speed v_T. A detailed analysis of the size-scaling properties of Eqs. (15) and (16) for nominal openings can be carried out assuming that $\Sigma_0^{\text{new}} = \sigma^2 \Sigma_0^{\text{old}}$ and the following scaling properties on the variables involved in Eq. (8): $t_{\text{ep}} \propto \sigma$, given that t_{ep} is directly proportional to a parachute's chord; $D \propto 1/\sigma^2$, given that $D \propto 1/\Sigma_0$; and $v_T \propto 1/\sigma$, given that $v_T \propto 1/\Sigma_0^{0.5}$. Implementing these proportions into Eqs. (15) and (16) gives the curve shown in Fig. 10, which relates the maximum acceleration ratio $a_{\max}^{\text{chute2}}/a_{\max}^{\text{chute1}}$ to the scale factor σ. Here the reference parachute (labeled chute 1) is characterized by the parameter set characterizing the standard brake setting of the Sabre 150 discussed earlier: $v_0^{\text{old}} = 125$ ft/s, $\Sigma_0^{\text{old}} = 20$ ft^2, $v_{ff} = 176$ ft/s, $t_{\text{ep}}^{\text{old}} = 1.18$ s, $w = 205$ lb, and $\rho = 0.00211$ sl/ft^3. Figure 10 shows that for most values of the scale factor, smaller parachutes actually open harder than the larger ones, a trend that is opposite to that of instant openings. For small-enough scale reductions, however, the opening shock reverses the trend and decreases at smaller σ, a result of having a parachute generating little drag area from that point on. On the other hand, the large-σ limit of the curve displayed is given by

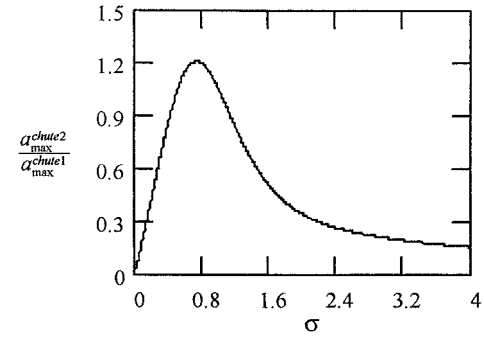

Fig. 10 Maximum acceleration ratio vs linear dimension scale.

$$(a_{\max})_{\text{chute2}} \approx (1/\sigma)\left[(-v_T/v_0)^{1.992}(a_{\max})\right]_{\text{chute1}} \tag{19}$$

which for $t_{\max}$ corresponds to

$$(t_{\max})_{\text{chute2}} = \sigma^{0.062}\left[(v_0/-v_T)^{1.12}(t_{\max})\right]_{\text{chute1}} \tag{20}$$

One can use the data of Fig. 10 on the Sabre 120, which sizewise is a scaled down version of a Sabre 150, by a factor $\sigma \sim (120/150)^{0.5} \sim 0.89$; here one calculates $a_{\max}^{120}/a_{\max}^{150} = 1.13$ and $v_0^{120}/v_0^{150} = 1.12$, which is quite consistent with the averaged experimental data shown in Figs. 5–8.

Scaling with Respect to the Canopy Spreading Rate Constant K

Scaling at fixed payload weight and initial speed v_0 can be derived similarly. When chute 1 and chute 2 are defined as jumps performed with parachutes of different designs, Eqs. (11) and (12) yield

$$\left[\frac{a_{\max}}{(\rho \cdot K)^{0.332}}\right]_{\text{chute2}} = \left[\frac{a_{\max}}{(\rho \cdot K)^{0.332}}\right]_{\text{chute1}} \tag{21}$$

$$\left[t_{\max} \cdot (\rho \cdot K)^{0.354}\right]_{\text{chute2}} = \left[t_{\max} \cdot (\rho \cdot K)^{0.354}\right]_{\text{chute1}} \tag{22}$$

thereby suggesting a mild dependence on the spreading rate.

These scaling laws, and the multitude of others that can be derived at fixed K, provide ways of studying parachute inflation dynamics without the explicit knowledge of K. These laws should also complement existing scaling formulas pertaining to a ram-air parachute glide performance[19,40] and provide a good basis for engineering design.

Conclusions

This paper has shown that the IPM provides good modeling possibilities for the study of manned, slider-reefed, ram-air parachute inflation. Our database shows clearly the strengths of the model, namely, its good prediction capability for $a_{\max}$ and $t_{\max}$. The IPM is also simple and yet detailed enough to produce several scaling laws that can be directly tested by experiment and subsequently used in prototype design.

Acknowledgments

The authors are grateful to Performance Designs, Inc., and to the U.S. Bureau of Land Management for providing financial support as well as loaning and rigging the test canopies for this project. The authors thank W. Coe and W. Downey from Performance Designs, Inc., for fruitful discussion and support.

References

[1]Butler, M., and Crowe, M., "Design, Development and Testing of Parachutes Using the BAT Sombrero Slider," AIAA Paper 99-1708, June 1999.

[2]Knacke, T. W., "Parachute Recovery Systems Design Manual," Para Publishing, Santa Barbara, CA, 1992.

[3]Peterson, C. W., Higuchi, H., and Strickland, J. H., "The Fluid Dynamics of Parachute Inflation," *Annual Review of Fluid Mechanics*, Vol. 28, Annual Review Inc., Palo Alto, CA, 1996, pp. 361–387.

[4]Wolf, D. E., "A Simplified Dynamic Model of Parachute Inflation," *Journal of Aircraft*, Vol. 11, No. 1, 1974, pp. 28–33.

[5]McVey, D. F., and Wolf, D. E., "Analysis of Deployment and Inflation of Large Ribbon Parachutes," *Journal of Aircraft*, Vol. 11, No. 2, 1974, pp. 96–103.

[6]Macha, J. M., "A Simple Approximate Model of Parachute Inflation," AIAA Paper 93-1206, May 1993.

[7]Purvis, J. W., "Theoretical Analysis of Parachute Inflation Including Fluid Kinetics," *Journal of Aircraft*, Vol. 19, No. 4, 1982, pp. 290–296.

[8]Purvis, J. W., "Prediction of Parachute Line Sail During Lines-First Deployment," *Journal of Aircraft*, Vol. 20, No. 11, 1983, pp. 940–945.

[9]Potvin, J., "Simple Description of Airflow Characteristics Inside an Unfolding Parachute," *Journal of Aircraft*, Vol. 36, No. 5, 1999, pp. 809–818.

[10]O'Hara, F., "Notes on the Opening Behavior and the Opening Forces of Parachutes," *Journal of the Royal Aeronautical Society*, Vol. 53, No. 3, 1949, pp. 1053–1062.

[11]French, K. E., "Inflation of a Parachute," *AIAA Journal*, Vol. 1, No. 11, 1963, pp. 2615–2617.

[12]Heinrich, H. G., "Opening Time of Parachutes Under Infinite-Mass Conditions," *Journal of Aircraft*, Vol. 6, No. 3, 1969, pp. 268–272.

[13]Payne, P. R., "A New Look at Parachute Opening Dynamics," *Aeronautical Journal of the Royal Aeronautical Society*, Vol. 75, 1973, pp. 85–93.

[14]Lingard, J. S., "A Semi-Empirical Theory to Predict the Load-Time History of an Inflating Parachute," AIAA Paper 84-0814, April 1984.

[15]Garrard, W. L., "Application of Inflation Theories to Preliminary Parachute Force and Stress Analysis," AIAA Paper 91-0862, April 1991.

[16]Ludtke, W. P., "A Technique for the Calculation of the Opening Shock for Several Types of Solid Cloth Parachutes," AIAA Paper 73-477, May 1973.

[17]Potvin, J., "Deployment Model for Slider-Reefed Ram-Air Parachutes," AIAA Paper 95-1564, May 1995.

[18]Potvin, J., "Testing a New Model of Ram-Air Parachute Inflation," *Aeronautical Journal*, Vol. 101, No. 1007, 1997, pp. 299–313.

[19]Lingard, J. S., "Ram-Air Parachute System Design," 2nd AIAA Aerodynamic Decelerator Systems Seminar, Unpublished, May 1995.

[20]Perschbacher, T., and Potvin, J., "The Improved Ideal Parachute Model and Its Application to the Inflation Dynamics of Slider-Reefed Ram-Air Parachutes and Round Parachutes," AIAA Paper 99-1750, June 1999.

[21]Potvin, J., Brocato, B., and Peek, G., "Experimental Validation of the Ideal Parachute Model: A Status Report," AIAA Paper 99-1746, June 1999.

[22]Strickland, J. H., and Macha, M., "Preliminary Characterization of Parachute Wake Recontact," *Journal of Aircraft*, Vol. 27, No. 6, 1990, pp. 501–506.

[23]Ludtke, W. P., "A Technique for the Calculation of the Opening-Shock Forces for Several Types of Solid Cloth Parachutes," *Proceedings of the 4th AIAA Aerodynamic Decelerator Systems Technology Conference*, AIAA, New York, 1973, pp. 176–185.

[24]Cockrell, D. J., and Haidar, N. I. A., " Influence of the Canopy-Payload Coupling on the Dynamic Stability in Pitch of a Parachute System," AIAA Paper 93-1248, May 1993.

[25]White, F. M., and Wolf, D. F., "Theory of Three-Dimensional Parachute Dynamic Stability," *Journal of Aircraft*, Vol. 5, No. 1, 1968, pp. 86–92.

[26]Doherr, K.-F., "Theoretical and Experimental Investigation of Parachute-Load-System Dynamic Stability," AIAA Paper 75-1397, 1975.

[27]Tory, C., and Ayres, R., "Computer Model of a Fully Deployed Parachute," *Journal of Aircraft*, Vol. 14, No. 7, 1977, pp. 675–679.

[28]Eaton, J. A., and Cockrell, D. J., "The Validity of the Leicester Computer Model for a Parachute with Fully-Deployed Canopy," AIAA Paper 79-0460, March 1979.

[29]Yavuz, T., and Cockrell, D. J., "Experimental Determination of Parachute Apparent Mass and Its Significance in Predicting Dynamic Stability," AIAA Paper 81-1920, Oct. 1981.

[30]Cockrell, D. J., and Doherr, K.-F., "Preliminary Considerations of Parameter Identification Analysis from Parachute Aerodynamic Flight Test Data," AIAA Paper 81-1940, Oct. 1981.

[31]Doherr, K.-F., and Saliaris, C., "On the Influence of Stochastic and Acceleration Dependent Aerodynamic Forces on the Dynamic Stability of Parachutes," AIAA Paper 81-1941, Oct. 1981.

[32]Eaton, J. A., "Added Mass and the Dynamic Stability of Parachutes," *Journal of Aircraft*, Vol. 19, No. 5, 1982, pp. 414–416.

[33]Cockrell, D. J., and Doherr, K.-F., "Preliminary Considerations of Parameter Identification Analysis from Parachute Aerodynamic Flight Test Data," AIAA Paper 81-1940, Oct. 1981.

[34]Lingard, J. S., "Effects of Added Mass on Parachute Inflation Force Coefficients," AIAA Paper 95-1561, May 1995.

[35]Heinrich, H. G., and Hektner, T. R., "Flexibility as a Model Parachute Performance Parameter," *Journal of Aircraft*, Vol. 8, No. 9, 1971, pp. 704–709.

[36]Potvin, J., Montanez, R., and Peek, G., "The Parks College Ram-Air Parachute Deployment Study: a Status Report," AIAA Paper 97-1426, June 1997.

[37]Potvin, J., Montanez, R., and Peek, G., "The Parks College Ram-Air Parachute Deployment Study," *Proceedings of the 1997 Parachute Industry Association International Symposium*, Feb. 1997.

[38]Potvin, J., and Peek, G., "The Parks College Parachute Research Group: Putting Science at the Service of Riggers and Manufacturers," *Proceedings of the 1999 Parachute Industry Association International Symposium*, Jan. 1999.

[39]Potvin, J., "Theoretical and Experimental Studies of Ram-Air Parachute Deployment Observable Variance," AIAA Paper 97-1544, June 1997.

[40]Goodrick, T. F., "Scale Effects on Performance of Ram Air Wings," AIAA Paper 84-0783, April 1984.